Available online at www.sciencedirect.com

ScienceDirect

Procedia IUTAM 26 (2018) 3–13

Procedia IUTAM

www.elsevier.com/locate/procedia

IUTAM Symposium Wind Waves, 4-8 September 2017, London, UK

Mechanisms And Modelling of Wind Driven Waves

J.C.R. Hunt[a], S.G. Sajjadi[b]

[a]*University College London, UK.*
[b]*Embry-Riddle Aeronautical University, Florida, USA.*

Abstract

This paper reviews (in qualitative and order of magnitude terms) the main mechanisms determining wind driven waves and their quantitative modelling for the different stages as the wind speed and the Reynolds number both increase, initially through coupling the instability 'waves' in the laminar boundary layers above and below the water surface, secondarily through initiation of eddy structures in turbulent boundary flow over flat water surface ('cats paws') and thirdly as distorted airflow passes over the undulating water surface with different kinds of dynamics, wave shapes (ranging from sinusoidal to pointed forms), amplitude H, wavelength L, travelling at speed c_r and growth rate c_i/U_*, coupled with the flow below the water surface. Significant flow features are the turbulent thin shear layers on the surface and detached 'critical' layers above the surface, which are also affected by the variation of surface roughness near the crests of the waves, by recirculating, separated flows near the surface and by high gradients of turbulence structure in the detached critical layers. Two phase flows in the recirculation zones on the lee side of waves leads to spray in the air above the water surface which also amplifies the boundary layer turbulence. Two phase bubbly flows below the surface generate near surface bubbles and may increases the surface drag downstream of the wave crests. The topology of node and saddle singular points in these mean recirculating flows provides a kinematic description of these flows. Idealised dynamical studies are presented of the variation of the wave amplitude through wind forces on waves moving in groups of waves, and thence physical models are proposed for the transfer of wave energy between large and small frequencies and length scales of wave spectra.

Peer-review under responsibility of the scientific committee of the IUTAM Symposium Wind Waves.

Keywords: Type your keywords here, separated by semicolons ;

1. Introduction

The basic forms of inertial-gravity waves are those that are produced at flat air-water surfaces by unsteady forces below the surface, the basic type being the waves driven by oscillating paddles in laboratory water tanks, that are initially unidirectional and monochromatic. These were first analysed by Stokes (see e.g. Lamb 1932). Different kinds of growing water waves on initially flat water surfaces are produced when air flow with mean velocity Uo passes over

* Corresponding author. Tel.: +0-000-000-0000 ; fax: +0-000-000-0000.
E-mail address: julian.hunt@ucl.ac.uk

2210-9838
Peer-review under responsibility of the scientific committee of the IUTAM Symposium Wind Waves.
10.1016/j.piutam.2018.03.002

the water surface, causing small viscous and larger turbulent shear stresses at the air-water interface which couple the air and water motions above and below this level (Hunt *et al.* 2010). The forms of these wind driven waves depend on the relative speed c_r/U, and the Reynolds number $Re = U_0 L/\nu$.

There are several stages in the non-linear development of these basic types of surface wave, which are associated with growing amplitude of the waves (defined by the ratio of their heights to lengths H/L) and their interactions.

As inertial-gravity waves grow in amplitude, provided viscous stresses are small (i.e. $Re \gg 1$), certain small fluctuations of wave shape develop and persist in the direction of the propagating wave. The most significant of these finite slope and persistent forms are 'fully non-linear Stokes' waves with steep crests and troughs with low slopes, (Longuet-Higgins 1978, Sajjadi 1988). The other kinds of non-linear waves are where there are two or more distinct types of wave with different wave lengths and frequencies, as discovered by Benjamin & Feir (1967). With larger amplitude and greater distances, these types of waves form wave groups with larger and smaller wave lengths travelling at different speeds. Following Hasselman (1962), Longuet-Higgins (1962), Phillips (1977) these interactions can be described by the changes to the energy spectrum of the waves. With further growth the interactions affect the gradients of the wave surface, and typically smaller breaking waves within larger groups (Longuet-Higgins & Turner 1974).

This paper first reviews briefly how small waves grow from small stresses into larger waves, and then for monochromatic and Stokes waves how the wave structure changes as a result of wind-wave interactions. Finally we consider how wave groups affect the wind structure over the waves, which can lead to a significant transfer of energy from the wind to the waves, their related turbulent boundary-layer flows, and thin recirculating shear layers close to and above the wave surfaces. Sharp variations in the distortion of turbulence also occur within and outside these layers. By extension, the study of these fluid-dynamical problems contributes to our fundamental understanding of mechanisms that occur in wave dominated environmental and engineering flows of many kinds. For example improvements to the modelling of wind -driven ocean waves have led to improved forecasts of ocean waves, which typically have global rms errors of 0.6 m (Fuller & Kellett 1997), which is only about 15-20% of the rms wave height. These errors increase systematically when large waves are forecast, when the waves are not forced locally by wind, and when the mean wind conditions are changing.

An important feature of turbulent boundary-layer flow over waves is that the boundary layer is distorted over a horizontal length scale, L, that is comparable to, or shorter than, the depth of the boundary layer, h, so that a large fraction of the depth of the boundary layer does not have time to come into equilibrium during the distortion. This significantly affects the turbulent stresses, as will be explained in section 3. In this paper we explain how various aspects of the changes in the flow over hills and waves vary across different parts of the flow by identifying the largest terms in the equations governing the mean dynamics, as well as the main mechanisms and timescales that govern perturbations to the turbulence. We also review the ways in which various approaches to modeling these aspects are being used for research and for practical problems involving environmental flows. Atmospheric flows are signicantly accelerated over the tops of waves and hills even when the maximum slopes are quite small, because shear in the approaching wind amplies this acceleration (Belcher & Hunt 1998).

The bulk effect of flow over waves is to increase the drag of the surface on the large-scale atmospheric motion. Some of the mean streamlines are determined both by the accelerating/decelerating wind over wave surfaces, and by recirculating flow in the wake regions. Furthermore, turbulence in the flow is greatly changed in the wake. Together these changes to the mean flow and turbulence affect mixing and exchange processes. Research and forecasting models of ocean waves have been guided by the theory of wind-wave generation proposed by Miles (1957) and by Hasselmanns(1962) theory of weakly nonlinear transfer of energy between waves of different wavelength (e.g. Komen *et al.* 1994). We highlight here recent research developments, including those that remain controversial.

Turbulent momentum transfer across a flat gas-liquid interface depends on the interactions between shear-free turbulence in the two regions (denoted as +, −) on either side of the nearly flat horizontal interface. These are controlled by mechanisms, which depend on the magnitudes of the ratios $s = \rho_+/\rho_-, \nu = \nu_+/\nu_-, \gamma = u_{0+}/u_{0-}$ of the densities and viscosities of the fluids and the r.m.s. velocities of the turbulence u_{0+}, u_{0-} above and below the interface (Belcher *et al.* 2005).

This study focuses on situations where γ is very large or very small, and where the interface is nearly flat, so that coupling between turbulence on either side of the interface is determined by viscous stresses. Linearized rapid-distortion theory (RDT) with viscous effects has been developed by extending the previous studies of shear-free

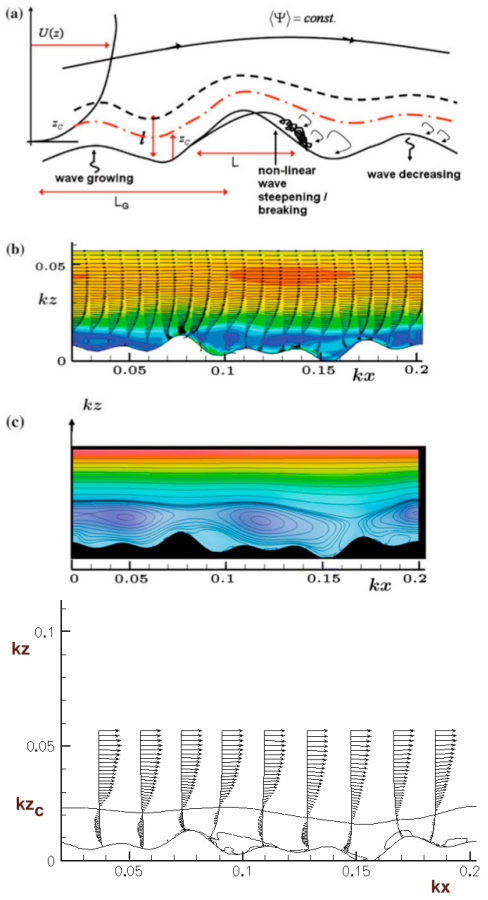

Fig. 1. From top to bottom: Top: (a) schematic of asymmetric wind flow over wave groups showing separation and changing behaviour of critical layer. Note the growing/decreasing wave amplitude in the group. This increases critical height $z_c(\ )$ on the downwind side of a group $\propto H$ where the wave shape changes. Second from the top (b) and second from the bottom (c): computations of turbulent flows over wave groups: (b) mean velocity, (c) mean streamlines relative to average velocity of the waves. Bottom: (d) unsteady critical layer and velocity vectors for (b) and (c).

turbulence near rigid plane boundaries, Hunt & Graham (1978), and over wavy surfaces (Belcher & Hunt 1992, Mastenbroek *et al.* 1996 and Ngata *et al.* 2006). The physical process also includes the blocking effect of the interface on normal components of the turbulence in 'source' layers and the viscous coupling of the horizontal field across thin interfacial viscous boundary layers. The horizontal divergence in the perturbation velocity field in the viscous layer also drives a weak inviscid irrotational velocity fluctuations outside the viscous boundary layers in a mechanism analogous to Ekman pumping.

As with other RDT analyses, the results are formally valid only over distortion times that are small compared with the Lagrangian time scales T_L. They show that

(a) the blocking effects are similar to those near rigid boundaries on each side of the interface, but through the action of the thin viscous layers above and below the horizontal and vertical velocity components differ from those near a rigid surface and are correlated or anti correlated respectively,

(b) the rapid growth of the viscous layers on either side of the interface is also significant so that the ratio of the r.m.s. values of the interfacial velocity fluctuations, u'_+ to that of the homogeneous turbulence far above the interface, u_0, does not vary with time. Note that if the turbulence is driven in the water then ($\gamma \ll 1$).

At the interface the horizontal straining is increased by the blocking, but decreases with time, and also the horizontal component of vorticity decreases with time. Where homogeneous turbulence is generated in the gas, at the shear-free gas-liquid interface ($\gamma \gg 1$), and the interface turbulence is given by $u'_I/u'_0 \sim 1/Re$.

(c) Non-linear interfacial effects are significant for times greater than T_L. When turbulence is generated in the liquid layer, it drives gas motions in the upper viscous layer at a high enough Reynolds number to generate turbulence. In the liquid the eddying motions are mainly determined by the linear blocking mechanism and u_{0+} is of the same order as u_{0-} as shown by Calmet & Magnaudet (2003); but at large times (e.g. in decaying turbulence) the vertical vorticity of the eddies dominates their structure near the interface as it is deformed by the growing viscous layer (Tsai *et al.* 2005).

When shear-free turbulence is generated in the upper layer and if the Reynolds number is less than about $10^6 - 10^7$ the fluctuations in the viscous surface layer do not become turbulent. However if additional fluctuations are stimulated in the lower layer by other mechanisms, such as mean shear, convection, waves, raindrops etc., the non-linear amplification leads to a more intense statistically steady state of turbulence in the liquid below the interface. Either for sheared or shear free turbulence in the gas, there is a large increase of the ratio of u'_I/u_{0+} to $s^{1/2} \sim 1/30$. This agrees with the direct numerical simulation of turbulent flow over a wavy wall reported by De Angelis *et al.* (1997). Even in this case (provided the surface is flat) the linear viscous coupling mechanism is still significant; for example, it ensures that the eddy motions on either side of the interface have a similar horizontal structure, although their vertical structure differs.

A number of mechanisms have been proposed for how air-flow over a horizontal body of liquid produces waves on its surface. Most of those proposed have been linear and therefore can be applied to any spectrum of waves. But the mechanisms and models based on them are regularly applied when the surface disturbances induce gas and liquid flows that are non-linear, and where the waves are not monochromatic. Typically the waves move in groups and the slopes of the water surface may become so large that the waves break and droplets form.

Very small unsteady waves are initiated by turbulence and/or growing Tollmien-Schlichting instabilities in the sheared air flow over the surface and Kelvin-Helmholtz coupled instability of the airflow over the liquid (Tsai *et al.* 2005). However, when steady waves are generated artificially in an airflow, e.g. in a wind-wave tank, the linear mechanisms for the growth of the waves are the pressure drag caused by asymmetric slowing of airflow over the downwind slopes of the waves and turbulence stresses caused by the disturbed flow, and wind-induced variations of surface roughness disturbed surface (Belcher & Hunt,1998). Both mechanisms are affected by the relative speed of the wave c_r to the friction velocity U_* of the airflow, and the disturbed flow changes at the critical height z_c, where the wave speed c_r is equal to the wind speed $U(z_c)$.

When the waves begin to grow at a significant rate kc_i, comparable with U_*k, the critical layer is above the inner shear layer near the surface, and the dynamics across the critical layer are determined by inertial forces as the flow accelerates and decelerates over the wave. If the wave is growing (or decaying), i.e. $|c_i| > 0$, and if the perturbation is finite there is a net force on the wave caused by critical layer dynamics (Belcher *et al.* 1999). But the integral inviscid analysis Miles (1957) for a growing wave, which was explained by Lighthills (1962) inviscid analysis and physical discussion showed that, even when $c_i \to 0$, there is apparently a finite drag force. However the computation of Sajjadi *et al.* (2014) showed that this inviscid limit is associated with an unphysical singular jet on the down-slope face of the wave (which have never been observed by experiments!). But for realistic viscous flows, critical layers of finite strength do form on the slopes and do contribute to the wind driven growth of the wave, typically when $c_i > 0$.

Nevertheless Miles inviscid result about the growth rate of monochromatic waves is still widely assumed to be the dominant mechanism for wind-wave momentum transfer and has been used to correlate data on the growth of wind-generated waves, and became the standard model for ocean wave forecasts (Janssen 2018).

An explanation is outlined below. In section 3 we analyse the combination of how realistic waves develop as a combination the inertial mechanism, and the wind drag mechanism acting together. The latter mechanism is based on the perturbation sheltering theory and computation by Belcher & Hunt (1992) and Mastenbroek *et al.* (1996), which assume c_r is small. But both models under estimate the energy-transfer parameter (being proportional to the wave growth) when c_r is comparable with the mean wind speed, because it does not represent the dynamics of realistic waves which grow and decrease in groups. Analytical models of steadily moving wave-group dynamics have been developed for the laminar/turbulent shear flow (Sajjadi *et al.* 2016), see also by McIntyre (1992).

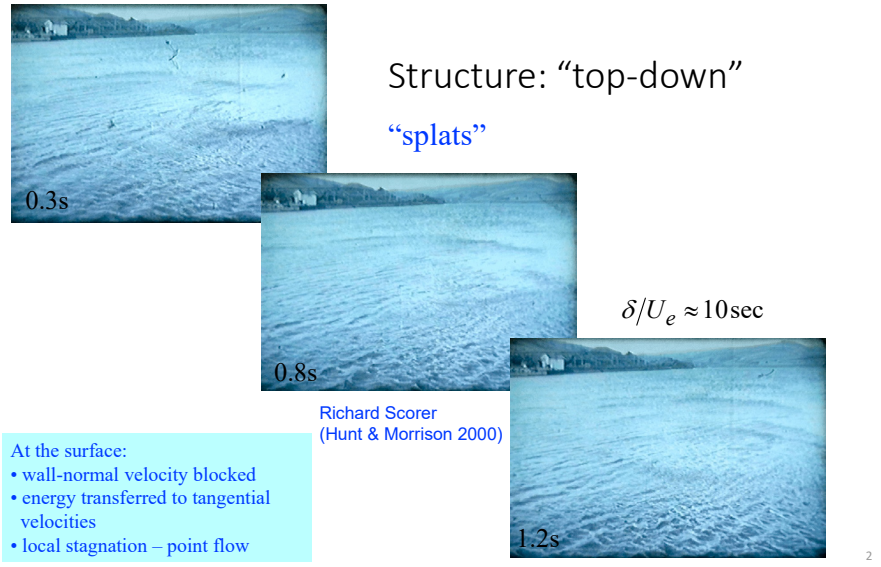

Fig. 2. Turbulent flow in the atmosphere over a flat surface generating ripples and showing gust structure - or ‘cats paws’ (Ref R.S.Scorer in Hunt & Morrison 2000)

Quasi-linear theory shows how individual waves in the group interact with the combined effects of the unsteady critical layer flow, and the viscous /turbulent sheltering on the lee sides of the waves. This wave group analysis can be extended and applied quantitatively or qualitatively to many environmental and industrial problems, and also to estimating heat and mass transfer. Thence by using weakly non-linear theory to analyse the disturbed air flow over the waves in groups, it is shown how the air flow over the downwind part of the group is slower than over the upwind part. This asymmetry causes the critical layer height to be higher where the waves slope downwards. This leads to the critical layer group (CLaG) effect producing a net horizontal force on the waves, in addition to the sheltering effect associated with monochromatic waves. This analysis, which is supported by numerical simulations (Sajjadi *et al.* 2018), shows why the critical layer is present over monochromatic waves but does not produce a net force, despite earlier arguments to the contrary.

Other wave-wind dynamics also affect the wave growth. Whether, as in the photographs by Jeffreys (1925) of wave groups of capillary waves on a Cambridge duck pond or breaking rollers in the Atlantic ocean, the wave shapes as well as their height vary in a group, with their slopes increasing downwind. This is likely to amplify the CLaG mechanism. By considering the dynamics of typical wave groups, it becomes possible to estimate rationally how air flow affects the non-linear interactions between waves, and compare how this relates to the wave-wave hydrodynamic interactions, that are assumed to dominate the distribution of ocean waves. For example variations of wave shapes within a group can also affect the net wave growth (Sajjadi *et al.* 2016) while violent erratic winds can prevent the formation of wave groups, so that wave growth may be reduced. This is observed in the downwind parts of wave groups located near the centre of hurricanes.

Wave group dynamics are particularly affected are also affected by the critical layers when they are located above the surface shear layer (i.e. $c_r > U_*$), where they can act to reduce the sheltering mechanism and reduce the drag

(Sajjadi *et al.* 2018). This contrasts with the upward trend of the drag of slower waves (when $c_r < U_*$) because the critical layer is now located within the shear layer, which increases the sheltering mechanism. Thus the decrease of the growth rate as c_r/U_* increases is partly compensated by the increase in growth rate as waves form into groups at higher wind speeds (which also needs to be modelled). This trend is also limited by the decrease in the sheltering mechanism as z_c increases over the downwind part of a wave group. Moreover, as $c_r = U_*$ increases the cat's-eye becomes larger and become significantly asymmetrical, with a stronger reverse flow below them, see (Sajjadi *et al.* 2014 and 2018).

Mean shear flows above and below gas-liquid interfaces generate turbulence with length scales of the order of that of the shear layer thickness h. Unstable buoyancy fluxes further increases the turbulent energy. But as two dimensional waves, moving parallel to the mean flow, develop on the liquid surface, the turbulence production is increased, through stretching of the vortex lines of the turbulent eddies (Texeira & Belcher 2002). But if elongated eddies are present, their longitudinal component of vorticity is systematically stretched as the flow moves over and under the waves, and steady roll structures are generated in the down wind direction (Belcher & Hunt 1998) These structures are observed in the air flow over rigid wavy surfaces in wind tunnels (Gong *et al.* 1996). Note also that low frequency, low wave number eddy motion can amplify the heat transfer between the gas flow and the surface, e.g. by 20% in the atmosphere Smedman *et al.* (2007). Recirculating and regular Langmuir patterns below liquid wavy surfaces are also driven significant gas shear flow U_* above the surface (Craik & Leibovich 1976) and (Sajjadi & Longuet-Higgins 2017). Their scalar transfer properties are also significant. These organised rolls above or below the surface are non-linearly amplified (i.e. increasing as their strength u/r increases relative to the mean flow) by the presence of the turbulence. As explained by Townsend (1976), extra turbulence is generated where the motions in the rolls impinge on the resistive surface, and less where the motions leave the surface, thus producing stresses parallel to the surface which further drive the roll motions. This explains why extra turbulence ($\sim w_*$) produced by buoyancy below the interface also amplifies the strength of rolls until $w_* > u/r$. Shorter and less coherent roll structures also form on the scale of the waves' lengths if the gas flow amplifies the surface waves sufficiently that they become three-dimensional, (Komori *et al.* 1993, Hunt *et al.* 2003)

2. Various mechanism related to air-sea interactions

We now review some of the mechanisms governing air-sea interface for ideal, non-ideal and group of waves.

2.1. Initial growth of wind driven waves

The growth of fluctuations in low wind speed flows over smooth water surfaces is the mechanism for how waves begin to grow, as shown for by the idealised inviscid flows of Kelvin-Helmholtz model (Lamb 1932). But for realistic, laminar viscous-inertial flows, where the Reynolds number is close to its critical value, the dynamical balance matches smoothly growing, sinusoidal fluctuations grow above and below air water surface Tsai *et al.* (2005) which are similar to the original one sided boundary layer fluctuations on a plane surface.

However when the Reynolds number significantly exceeds the critical value, the atmospheric boundary layer becomes fully turbulent, with characteristic eddy structures (with cats' paws growing as they cause ripples on the surface) and which are associated with well defined, self-similar spectra for large and small length scales. (Hunt & Morrison 2000). In particular the stream-wise wind energy spectrum has the form $kE_{11}(k) \sim U_*^2$, where U_* is the mean friction velocity. These eddy structures are associated with growing wind and pressure fluctuations leading to the growth of wind waves (Phillips 1977). These fluctuations near the water surface disturb the mean profile, as defined by the roughness length z_0.

The dynamics and thermodynamics of the small scale turbulence over wind driven waves are also changed when spray droplets and bubbles are generated above and below the water surface. These changes are especially significant for high intensity Tropical Cyclone winds, (where field measurements were performed by Lixiao *et al.* 2015), and laboratory measurements in a wind-wave tunnel by Iwano *et al.* (2013).

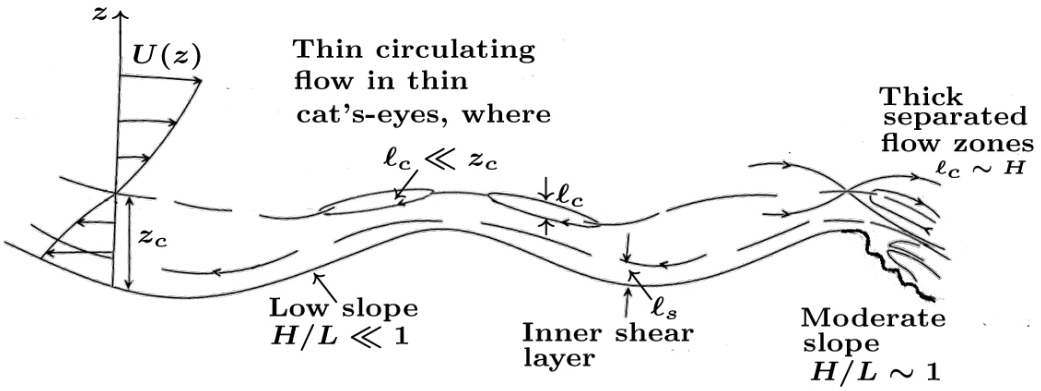

Fig. 3. Schematic diagram showing quasi-steady structure of mean streamlines over wind driven waves, for low and moderate slopes, at high wave speed $c_r \gg U_*$.

2.2. *Turbulent wind over wave trains*

We first consider the turbulent boundary layer above the air-water interface that generates low amplitude,($H \ll L$) travelling waves (with speed c_r) with very low growth rate i.e. $c_i \ll c_r \ll 1$, where

$$\Delta z = H(\exp[ik(x - c_r t) + kc_i t])$$

(see Fig 2). A thin surface shear layer forms with thickness $\ell \sim L/10$, As it passes over the wave surface. Near the surface, the mean profile is disturbed by variations of the surface roughness $z_0(\ll \ell)$ over the wave, typically reaching a maximum near the peak height of the wave surface (Gent & Taylor 1976). This critical cats-eye layer also forms at height z_c where the wind speed is equal to the wave speed, i.e.

$$U(z_c) - c_r = (U_*/\kappa)\ln(z_c/z_0) - c_r = 0.$$

When $z_c < \ell$ (as shown in Fig 2) the thickness ℓ_c of the critical layer is of order z_c, (and much larger than z_0). The phase-averaged turbulent shear stress and inertial dynamics within the surface layer matches the mean distorted flow outside the shear layer, which is determined both by the rapidly distortion eddies and by the inviscid field. Both the inner and outer flow contribute to determine the drag force on the wave surface. Either asymptotic multi-layer turbulence analysis, (Belcher & Hunt 1998), based on the original laminar 'triple deck methods' (Stewartson 1974) or complex Reynolds stress computation methods (Townsend 1972, Sajjadi *et al.* 2001) are used for quantitative results.

Note that at higher wave speeds, when the critical layer is located outside the inner shear layer, i.e. $z_c > \ell$, and the thickness ℓ_c of the layer is less than z_c. The critical layer tends to reduce mean vertical motions below the critical layer – a 'blocking effect'. The analysis by Belcher *et al.* (1999) shows that the drag force on the wave and its growth rate of the waves β tends to decrease as c_r/U_* increases.

3. Growing wave trains and breaking waves

Generally wind forces lead to the growth over time, or distance, of the amplitude H, length L and slope of the waves H/L, resulting from the balance of forces, at, above, and below the surface. The growth also tends to change the shape

of the waves, generally making slopes sharper near the crests and flatter near the troughs. Also, through fundamental instabilities, initially two-dimensional wave trains become three-dimensional. These overall developments also depend on the turbulent shear layer structure of the flow, both above and below the air-water surface, see Fig 3.

Physical understanding of these factors benefits from studies of relations between these general developments, and on improved modelling. For slow wave trains, i.e. $z_c < \ell$, moving with moderate to high slope, i.e. $H/L \gtrsim 1$, separated recirculating flow occurs on the lee slope (Figs 2 and 3). But if $H/L \sim 1$, and the waves are in the form of isolated two or three dimensional structures, then the recirculating wake flows can extend over a significant down wind distance (Jeffreys 1925).

Where waves travel at faster speeds, the elevations of the critical layers increase (i.e. $z_c > \ell$); they also grow in height H and length L, leading to separate and significant recirculating flows developing in the critical layer largely above the lee side, see Fig 3. Conditional sampling (e.g. relative to the maximum height of the wave) shows the distinction between the recirculating flows within the critical layer and separately in the recirculating shear layers that extends above and below the lee-side water surface.

For higher wind speeds, two phase flow physics is needed to model recirculating layers above the water surface which contain droplets and spray.While below the air-water surface there are bubbles produced by air entrained by the breaking wave. These distinct flow patterns were observed in gas-liquid turbulent flow in a pipe by Ayati *et al.* (2016). A new approach for modelling the interface between the highly turbulent shear layer near the water and

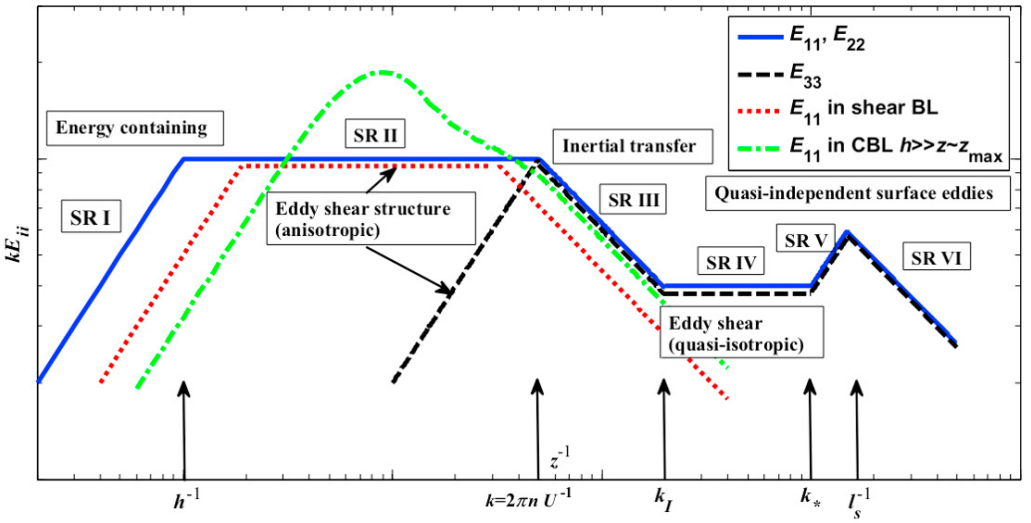

Fig. 4. Spectra of three-dimensional turbulent wind structure in a Tropical Cyclone over coastal area showing small scale energy from spray/wave process (Lixao, *et al.* 2015).

the weaker turbulence in the atmospheric boundary layer could be based on the phase averaged velocity profiles across the high-low intensity turbulent interfaces of separated aerofoil wakes-with application to the eddy wake structure of separated/breaking waves (Szubert *et al.* 2015). Following Lighthill (1963) and Hunt *et al.* (1978), the patterns of these conditionally sampled recirculating mean flows are defined by the points where the local flow is stationary, and defined topologically by saddle point and nodal points, as shown in Fig 3. These 'singular' points can be located in the air and/or water flow (Banner & Melville 1976). Fig 3 also shows how the surface shear stress and the plunging motion of fluid lumps in breaking waves drive the mean recirculation flow below the lee slope (Hunt *et al.* 2003). This process not only amplifies the turbulence and mean shear below the water surface, but also amplifies the streamwise Langmuir circulations, that can reduce the spanwise extent of waves on the surface (Belcher *et al.* 2012).

4. Wind effects on wave groups

Since laboratory driven waves (e.g. Benjamin & Feir 1967), as confirmed by wind driven waves, show that when the amplitude and wave length of monochromatic wave trains exceed a critical level, inertial-buoyancy forces induce wave trains to form into wave groups with amplitude H_G and overall length L_G, while the smaller amplitudes H_C of the component waves rise and fall as they travel through the group. The average speeds of the wave groups C_G are significantly smaller than the average speed C_c of the individual waves within the group (typically about $2C_G$). In such groups the wind flow and surface forces, on the scale of the group L_G, are significantly affected by the amplification and diminution of the wind waves within the group, notably by differing upwind and downwind of the maximum waves. The key point is that because the speed of the component waves within the group $u_{r,C}$ exceeds the wind speed U over the waves in the group, the height of the critical layer z_c exceeds the height of the surface shear layer ℓ.

However unlike the wind over steadily moving monochromatic waves (as analysed in previous sections), the perturbed wind flow above the critical layer (i.e. $z_c > \ell$) increases in amplitude over the component waves on the upwind side of the group over the component waves.They are travelling over the wave at a frequency c_i/L, where typically $c_i \ll U_*$. The amplitudes of the maximum of the wind speed over these unsteady waves in the critical layer at z_c, shown in Fig 1, are larger than for the steady air flow described in section 2.

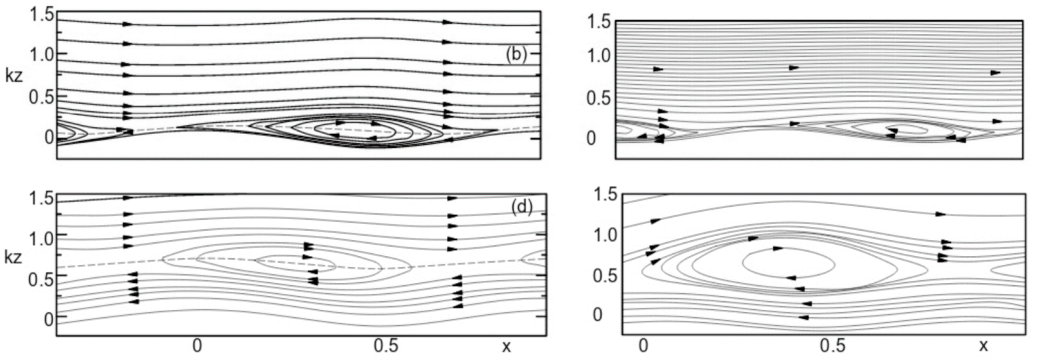

Fig. 5. Phase-averaged streamlines over stationary and moving waves with steepness 0.1. (b) $c/U_* = 3.9$; (d) $c/U_* = 11.5$. The dotted line corresponds to the height of the critical layer where $\langle u \rangle + u_w = 0$. Left diagrams from Sullivan's *et al.* (2000); right diagrams from Sajjadi *et al.* (2017).

But, as shown in Fig 1, on the downwind side of the group in the outer flow (above the critical layer) the mean wind flow is decelerating; also above the critical layer the amplitude of the component waves decrease. This is the reverse of the mechanism that amplifies outer wind speed on the upwind side. But, although there is an overall wind drag produced by the wind over the wave group, the average acceleration of the outer wind flow exceeds the deceleration downwind of the crest of the wave group. This also implies that there is net transfer of large scale wave energy over the scale of the wave group to the energy of the smaller scale 'component' waves within the wave group. This is an idealised analysis for how the different wave lengths and wave amplitudes contribute to the wind-wave process for the transfer between the energy of different spectral components of water waves and the wind field.

Quantitative estimates of the wave group mechanisms can be derived from critical layer dynamics using the eddy viscosity ν_e in the flow at and above the component critical layer $z_{c,C}$. Sajjadi *et al.* (2014) This shows how the component of the perturbed horizontal wind speed $u_{r,C}(x, z)$ is in phase with the deflection of the wave surface and has the profile of a mixed (or tanh) shear layer. This does not affect the net drag (Fig 5). But the wind speed component that is out of phase $u_{i,C}(x, z)$ is in the form of a thin jet on the downwind face of the component wave located at the critical layer height, and leads to the net drag. Alternatively, using the inviscid integral analyses by Miles (1957), Lighthill (1962) the explicit form of the net drag of the 'component' waves in the group can be derived (proportional to the property of the mean profile *viz* $U''(z_c)/(U'(z_c))^3$. Following the explanation in section 3, and Fig 4, the wind wave energy multi-scale transfer process also depends on two phase surface level energy transfer and subsurface turbulence (e.g. Phillips 1977, Hunt *et al.* 2003).

5. Conclusions

This paper has firstly reviewed the characteristic flow of monochromatic wind driven gas-liquid waves in relation to the qualitative and statistical structure of the mean and turbulent air flow above and below the water surface. A key feature of the development of the waves is the changing structure of separate layers with varying inertial and turbulent shear layer dynamics, depending on their Reynolds number and amplitude and length variations. Dissipative processes are an essential part of the dynamics when the wave growth is small. Analytic asymptotic solutions for these layers have been derived which are in the forms of quasi-steady and time dependent perturbations both near the turbulent surface shear layer and in the separate recirculating flows in detached critical layers. Variation of surface roughness also affects shear layers over the waves, which contributes to wave growth. Computation of non-linear turbulent and recirculating flows using new approaches, such as conditional sampling and modal analysis near sharp interfaces, are features of the overlapping flow structures such as recirculating separated flows and turbulent critical layers. We emphasize that the existence of a critical layer over a monochromatic with a significant dynamical role still does not mean that the Miles inviscid mechanism is operative, (Sullivan *et al.* 2000).

The second broad conclusion is that when there is significant growth of wind waves, this is significantly increased when the waves are formed into groups. In this common situation, inviscid theory (built on the Miles and Lighthill concepts) leads to growing individual waves on the upwind part of the wave group and reducing waves downwind of the peak of the wave group (Fig 1). This process leads to a net growth of waves if dissipation processes in the surface shear layers are included approximately in the model. Numerical simulations of wind over wave groups also show positive transfer wind energy to the wave groups. Wave groups are also significant when large and small waves shapes have sharp peaks – as is visible in the wave photograph in Sajjadi *et al.* 2014. This requires further research.

Topological description of critical points are shown to be effective in description and analysis of these different flow regions. These methods can be applied for showing how wind drag forces affect the interactions between larger and smaller waves, and thence can lead to a more physical model for wind effect on wave spectra (Phillips 1977).

Acknowledgements. SGS would like to thank the Trinity College, Cambridge, for their support as a visiting research fellow in the course of this research. We also are grateful for fruitful conversations with P. Janssen, R. Grimshaw and T. Johnson.

References

1. H. Lamb 1932. *Hydrodynamics*. Cambridge University Press. Cambridge.
2. M.S. Longuet-Higgins 1978. On the Dynamics of Steep Gravity Waves in Deep Water. In book: *Turbulent Fluxes Through the Sea Surface, Wave Dynamics, and Prediction*. DOI 10.1007/978 – 1 – 4612 – 9806 – 9 – 14.
3. S.G. Sajjadi SG 1988. Shearing flows over Stokes waves. Department of Mathematics Internal Report, Coventry Polytechnic, UK.
4. T.B Benjamin and J.E. Feir 1967. The disintegration of wave trains on deep water. Part 1. Theory. *J. Fluid Mech.* **27**, 417–430.
5. K. Hasselmann 1962. On the non-linear transfer in a gravity wave spectrum. Part 1. General theory. *J. Fluid Mech.* **12**, 481–500.
6. M.S. Longuet-Higgins 1962. Resonant interactions between two trains of gravity waves. *J. Fluid Mech.* **12**, 321–332.
7. O.M. Phillips 1977. *Dynamics of the upper ocean*. Cambridge University Press.
8. M.S. Longuet-Higgins and J.S. Turner 1974. An "entraining plume" model of spilling breaker. *J. Fluid Mech.* **63**, 1–20.
9. S. Fuller and M.Kellett 1997. *Annual Forecast Verification Statistics 1996*. Bracknell, UK: Meteorological Office.
10. S.E. Belcher and J.C.R. Hunt 1998. Turbulent flow over hills and waves. *Annu. Rev. Fluid Mech.* **30**, 507–538.
11. J.W. Miles 1957. On the generation of surface waves by shear flows. *J. Fluid Mech.* **3**, 185–204.
12. G.J. Komen, L. Cavaleri, M.A. Donelan, K. Hasselmann, S. Hasselmann and P.A.E.M. Janssen 1994. *Dynamics and modelling of ocean waves*. Cambridge University Press, Cambridge.
13. S.E. Belcher, J.N. Hacker and D.S. Powell 2005. Constructing design weather data for future climates. *Building Services Engineering Research And Technology*, **26**, 49-62.
14. J.C.R. Hunt and J.M.R. Graham 1978. Free-stream turbulence near plane boundaries. *J. Fluid Mech.* **84**, 209-235.
15. S.E. Belcher and J.C.R. Hunt 1993. Turbulent shear flow over slowly moving waves. *J. Fluid Mech.* **251**, 109-114.
16. C. Mastenbroek, V.K. Makin, M.H. Garat and J.P. Giovanangeli 1996. Experimental evidence of the rapid distortion of turbulence in air flow over waves. *J. Fluid Mech.*, textbf318, 273-302.
17. K. Nagata, H. Wong, J.C.R. Hunt, S.G. Sajjadi and P.A. Davidson 2006. Weak mean flows induced by anisotropic turbulence impinging onto planar and undulating surfaces. *J. Fluid Mech.*, textbf556, 329-360.
18. I. Calmet and J. Magnaudet 2003. Statistical structure of high-Reynolds-number turbulence close to the free surface of an open-channel flow. *J. Fluid Mech.*, textbf474, 355-378.

19.Y.S. Tsai YS, A.J. Grass and R.R. Simons 2005. On the spatial linear growth of gravity-capillary waves sheared by a laminar flow. *Phys. Fluids*, **17**, 95-101.
20.V. De Angelis, P. Lombardi, and S. Banerjee 1997. Direct numerical simulation of turbulent flow over a wavy wall. *Phys. Fluids*, **9**, 2429. Physics of Fluids 9, 2429 (1997)
21.S.E. Belcher, J.C.R. Hunt and J.E. Cohen 1999. Turbulent flow over growing waves. In *Proceedings of IMA Conference on Wind Over Waves*. Sajjadi, S.G., Thomas, N.H. and Hunt, J.C.R. (eds). Oxford University Press, pp. 19–30.
22.M.J. Lighthill, M.J. 1962. Physical interpretation of the theory of wind generated waves. *J. Fluid Mech.*, **14**, 385–398.
23.S.G. Sajjadi, J.C.R. Hunt and F. Drullion 2014. Asymptotic multi-layer analysis of wind over unsteady monochromatic surface waves. *J. Eng. Math.*, **84**, 73–85.
24.P.A.E.M. Janssen and J-R. Bidlot 2018. Progress in operational wave forecasting. In: *IUTAM Symposium Wind Waves*, 4–8 September 2017, London, UK.
25.S.G. Sajjadi, J.C.R. Hunt and F. Drullion 2016. Growth of unsteady wave groups by shear flows, *Proc. of IMA Conference on Turbulence, Waves and Mixing*, S.G. Sajjadi and H.J.S. Fernando (eds). IMA Press, 79–84.
26.M.E. McIntyre 1992. On the role of wave propagation and wave breaking in atmosphereocean dynamics. In: *Proceedings of the 18th international congress theoretical and applied mechanics*, Haifa. Elsevier, Amsterdam, pp 281–304.
27.S.G. Sajjadi, J.C.R. Hunt and F. Drullion 2018. Computational turbulent shear flows over growing and non-growing wave groups In: *IUTAM Symposium Wind Waves, 4–8 September 2017, London, UK*.
28.H. Jeffreys 1925. On the formation of water waves by wind. *Proc. R. Soc. Lond.* A **107**, 189-206.
29.M.A.C. Teixeira and S.E. Belcher 2002. On the distortion of turbulence by a progressive surface wave. *J. Fluid Mech.*, **458**, 229-267.
30.W.M. Gong, P.A. Taylor and A. Dornbrack 1996. Turbulent boundary-layer flow over fixed aerodynamically rough two-dimensional sinusoidal waves. *J. Fluid Mech.*, **312**, 1-37.
31.A. Smedman, U. Högström, J.C.R. Hunt and E. Sahlée 2007. Heat/mass transfer in the slightly unstable atmospheric surface layer. *Q.J. Roy. Met. Soc.*, **133**, 622.
32.A.D.D. Craik and S. Leibovich 1976. A rational model for Langmuir circulations. *J. Fluid Mech.*, **73**, 401-426.
33.S.G. Sajjadi and M.S. Longuet-Higgins 2017. Instability of Langmuir circulations by wind. *Adv. Appl. Fluid Mech.* **19**, 725–763.
34.A.A. Townsend 1976. *The Structure of Turbulent Shear Flow*, 2nd edn., Cambridge University Press.
35.S. Komori, R. Nagaosa, Y. Murakami 1993. Turbulence structure and mass transfer across a sheared airwater interface in wind-driven turbulence. *J. Fluid Mech.*, **249**, 161-183.
36.J.C.R. Hunt, I. Eames and S.E. Belcher 2003. Vorticity dynamics in the water below steep and breaking waves. Proc. *Wind over waves; IMA conference* September 2001. S.G. Sajjadi and J.C.R. Hunt (eds), Ellis Horwood.
37.J.C.R. Hunt and J.F. Morrison 2000. Eddy structure in turbulent boundary layers. *Eur. J. Mech. B.* **19**, 673–694.
38.L. Lixiao, A. Kareem, Y. Xiao, L. Song and C. Zhou 2015. A comparative study of field measurements of the turbulence characteristics of typhoon and hurricane winds. *J. of Wind Engineering and Industrial Aerodynamics*, 140, DOI10.1016/j.jweia.2014.12.008
39.N. Iwano, N. Takagaki, R. Kurose and S. Komori 2013. Mass transfer velocity across the breaking air-water interface at extremely high wind speeds. *Tellus* B **65**, 21341.
40.P.R. Gent and P.A. Taylor 1976. A numerical model of the air flow above water waves *J. Fluid Mech.*, **77**, 105-128.
41.K. Stewartson 1974. Boundary layers on flat plates and related bodies. *Adv. Appl. Mech.*, **14**, 145-239.
42.A.A. Townsend 1972. Flow in a deep turbulent boundary layer over a surface distorted by water waves. *J. Fluid Mech.*, **55**, 719-735.
43.S.G. Sajjadi, T.J. Craft and Y. Feng 2001. A numerical study of turbulent flow over a two-dimensional hill. *Int. J. Numer. Methods Fluids*, **35**, 1-23.
44.S.G. Sajjadi, J.C.R. Hunt and F. Drullion 2017. Turbulent shear flows over smooth or peaked, and steady or unsteady monochromatic water wave. *J. Fluid Mech.*, to appear.
45.D. Szubert, F. Grossi, A.J. Garcia, Y. Hoarou, J.C.R. Hunt and M. Braza 2015. Shock-vortex shear-layer interaction in the transonic flow around a supercritical airfoil at high Reynolds number in buffet conditions. *J. Fluids Struct.*, **55**, 276-302.
46.J.C.R. Hunt, T. Ishihara, D. Szubert, I. Asproulias, Y. Hoarau and M. Braza 2016. Turbulence Near Interfaces-Modelling and Simulations M. Braza *et al* (eds.) Advances in Fluid-Structure Interaction, Notes on Numerical Fluid Mechanics and Springer Multidisciplinary Design 133, DOI 10.1007/978 – 3 – 319 – 27386 – 0 – 17, Springer.
47.M.J. Lighthill 1963. Attachment and separation in three-dimensional flows. In *Laminar Boundary Layers*, L. Rosenhead (ed). Ch. 2, pp. 72-82. Oxford University Press, Oxford.
48.J.C.R. Hunt, C.J. Abell, J.A. Peterka and H. Woo 1978. Kinematical studies of the flows around free or surface-mounted obstacles; applying topology to flow visualization. *J. Fluid Mech.*, **86**, 179-200.
49.M.L. Banner and W.K. Melville 1976. On separation of air flow over water waves. *J. Fluid Mech.*, **77**, 825-842.
50.S.E. Belcher, A.L.M. Grant, K.E. Hanley, B. Fox-Kemper, L. Van Roekel, P.P. Sullivan, W.G. Large, A. Brown, A. Hines, D. Calvert, A. Rutgersson, H. Pettersson, J.R. Bidlot, P.A.E.M. Janssen and J.A. Polton 2012. A global perspective on Langmuir turbulence in the ocean surface boundary layer. *Geophysical Research Letters*, **39** (L18605).
51.J.C.R. Hunt, S.E. Belcher, D.D. Stretch, S.G. Sajjadi, J.R. Clegg 2010. Turbulence and wave dynamics across gas-liquid interfaces. In: *Proceedings of the symposium on gas transfer at water surfaces*, S. Komori, R. Kurose (eds.) Kyoto, Japan.
52.P.P. Sullivan, J.C. McWilliams and C.H. Moeng 2000. Simulation of turbulent flow over idealized water waves. *J. Fluid Mech.*, **404**, 47–85.